# Deformation Mechanisms during Low- and High-Temperature Superplasticity in 5083 Al-Mg Alloy

I.C. HSIAO and J.C. HUANG

The controlling deformation mechanisms and grain boundary sliding behavior during low-, medium-, and high-temperature superplasticity (LTSP, MTSP, and HTSP) in fine-grained 5083 Al-Mg base alloys are systematically examined as a function of strain. Grain boundary sliding was observed to proceed at temperatures as low as 200 °C. With increasing LTSP straining from the initial ($\varepsilon < 0.5$) to later stages ($\varepsilon > 1.0$), the strain rate sensitivity $m$, plastic anisotropy factor $R$, high-angle grain boundary fraction, grain size exponent $p$, and grain boundary sliding contribution all increased. During the initial LTSP stage, there was little grain size dependence and the primary deformation mechanisms were solute drag creep plus minor power-law creep. At later stages, grain size dependence increased and grain boundary sliding gradually controlled the deformation. During MTSP and HTSP, solute drag creep and grain boundary sliding were the dominant deformation mechanisms.

## I. INTRODUCTION

SUPERPLASTIC forming of commercial low-priced aluminum, magnesium, and titanium sheets could be developed into one of the important future fabrication means for the automobile, train, architecture, and electronic appliance industries. There are at least three main factors that need to be considered: (1) the alloy itself is commercially widely available and cheap; (2) the forming rate is sufficiently high; and (3) the forming temperature is as low as possible. A higher forming rate to a strain rate greater than $10^{-2}$ $s^{-1}$ would satisfy the current fabrication speed,[1] while a lower forming temperature would save fabrication energy and prevent severe grain growth, cavitation, and solute-loss from surface layers, as well as maintain superior postform properties.[2] Following these guidelines, the development of superplastic Al-Mg, Al-Mg-Si, or Mg-Al-Zn base alloys has attracted attention lately, including experimental alloys such as Al-3Mg or Al-10Mg and commercial alloys such as AA5052, 5083, 6061, 6011, AZ91, AZ31, *etc*.

There have been numerous efforts in processing aluminum materials to exhibit high strain rate superplasticity (HSRSP) or low-temperature superplasticity (LTSP) by using thermomechanical treatments (TMT), equal channel angular extrusion (ECAE), multiple forging, cyclic extrusion, torsion under compression, or accumulative roll bonding (ARB)[3–14] on commercial or experimental alloys. In the beginning of the development of LTSP, the strain rate was typically less than $10^{-3}$ $s^{-1}$. Until the work by Valiev *et al.*[15] in 1997, the Al alloy exhibited not only low-temperature superplasticity but also high strain rate ($10^{-2}$ to $10^{-1}$ $s^{-1}$) superplasticity. Selected LTSP reports are summarized in Table I, where it can be seen that LTSP has been developed in Al, Mg, Zn, Ti, Ni, and Cu and intermetallic alloys over the past 10 years.[9,15,22–35]

In our previous studies,[26,36,37] a simple rolling-type TMT was applied to process the low-priced commercial 5083 alloy, resulting in low-temperature superplasticity at around 230 °C to 270 °C and $2 \times 10^{-4}$ to $1 \times 10^{-2}$ $s^{-1}$, with an optimum tensile elongation of 511 pct. The TMT processed thin sheet contained grains and subgrains measuring around 0.5 $\mu$m. At temperatures lower than 270 °C, the grains grew limitedly and maintained LTSP, with failure by cavitation coalescence plus partial necking. The flow stress of the LTSP specimens at 250 °C dropped to nearly one-half as compared with the as-received non-LTSP samples, and the strain rate sensitivity $m$ increased from 0.15 for the as-received specimens to around 0.3 to 0.35 of the LTSP ones. The grain-structure, texture, and grain-orientation evolutions as a function of strain, strain rate, and temperature have been presented previously.[36,37]

In this report, the possible controlling deformation mechanisms during LTSP loading are characterized and discussed. There have been very limited analyses on the deformation mechanisms for fine-grained LTSP materials.[2,27,38–40]. Pu *et al.*[2] suggested that viscous dislocation creep would control the flow of the LTSP 8090 Al alloy with stress exponent $n \sim 3$ and activation energy $Q$ close to pipe or grain boundary diffusion. However, Mabuchi *et al.*[27] claimed a grain size dependence that would not be consistent with solute drag viscous dislocation creep. Recently, for LTSP in Mg-base alloys and composites, $n$ has been reported to be 2[38] or 3,[39] the grain size exponent $p$ to be 2[38] or 3,[40] and $Q$ to be close to lattice diffusion[38] or grain boundary diffusion.[40] There seems to be no consensus on the acting mechanisms, and further analyses appear to be necessary. Questions that needed to be explored include the following: (1) Would grain boundary sliding (GBS) still operate at low temperatures around $(0.5 \pm 0.1)T_m$ (where $T_m$ is the melting temperature expressed in K)? (2) What are the controlling accommodation and diffusion steps during LTSP? (3) Would the controlling mechanism be changed over the LTSP straining process? (4) Would there be grain size dependence?

## II. EXPERIMENTAL METHOD

The 5083 alloy was obtained from CS Aluminum Corp., (Taiwan), in the form of hot-rolled 30-mm-thick plates, with

I.C. HSIAO, Postdoctoral Student, and J.C. HUANG, Professor and Chairman, are with the Institute of Materials Science and Engineering, National Sun Yat-Sen University, Taiwan 804, Republic of China. Contact e-mail: jacobc@mail.nsysu.edu.tw

Manuscript submitted September 18, 2001.

**Table I. Summary of Representative LTSP Reports in Fine-Grained Metallic Materials**

| Material | Processing | $d$ ($\mu$m) | Temperature (°C) | $\dot{\varepsilon}$ ($s^{-1}$) | Elongation | Reference |
|---|---|---|---|---|---|---|
| Al-10Mg-0.5Mn | TMT | — | 300 (0.61 $T_m$) | $1 \times 10^{-3}$ | 400 pct | 22 |
| Al-10Mg-0.1Zr | TMT | — | 300 (0.61 $T_m$) | $1 \times 10^{-3}$ | 1100 pct | 9 |
| Al-4Cu-0.5Zr | torsion | 0.3 | 220 (0.53$T_m$) | $3 \times 10^{-4}$ | 250 pct | 23 |
| Al-8090 | TMT | 0.7 | 350 (0.67$T_m$) | $8 \times 10^{-4}$ | 710 pct | 24 |
| Al-4Cu-0.5Zr | ECAE | 0.5 | 250 (0.56$T_m$) | $1 \times 10^{-4}$ | 850 pct | 25 |
| Al-5Mg-2Li-Zr | ECAE | 1.2 | 350 (0.67$T_m$) | $1 \times 10^{-2}$ | 1180 pct | 15 |
| Al-5083 | TMT | 0.5 | 230 (0.54$T_m$) | $2 \times 10^{-3}$ | 511 pct | 26 |
| Mg-AZ91 | ECAE | 1.0 | 200 (0.51$T_m$) | $6 \times 10^{-5}$ | 661 pct | 27 |
| Mg-ZK60/SiC | extrusion | 1.7 | 190 (0.50$T_m$) | $1 \times 10^{-4}$ | 350 pct | 28 |
| Zn-0.3Al | TMT | 1.0 | 25 (0.40$T_m$) | $2 \times 10^{-4}$ | 1400 pct | 30 |
| Zn-22Al | ECAE | 0.6 | 100 (0.50$T_m$) | $3 \times 10^{-4}$ | 450 pct | 29 |
| Ti-6Al-4V | torsion | 0.15 | 650 (0.46$T_m$) | $1 \times 10^{-2}$ | 305 pct | 31 |
| Ti-25Al | forging | 0.3 | 600 (0.44$T_m$) | $6 \times 10^{-4}$ | 300 pct | 32 |
| Ti-50Al | forging | 0.3 | 800 (0.57$T_m$) | $8 \times 10^{-4}$ | 355 pct | 33 |
| Ni | deposition* | 0.02 | 350 (0.36$T_m$) | $1 \times 10^{-3}$ | 300 pct | 34 |
| $Ni_3Al$ | torsion | 0.05 | 650 (0.55$T_m$) | $1 \times 10^{-3}$ | 375 pct | 34 |
| Cu | deposition* | 0.02 | 25 (0.22$T_m$) | $1 \times 10^{-3}$ | >1000 pct** | 35 |

*By high-purity electrodeposition technique.
**Deformed by room temperature rolling instead of tensile straining.

a composition of Al-4.7wtpctMg-0.7wtpctMn. The thick plates possessed elongated grains measuring $500 \times 80 \times 8$ $\mu m^3$ and did not exhibit any LTSP. An annealing treatment was performed at 500 °C for 1 hour, followed by air cooling, resulting in nearly equiaxed grains measuring ~25 $\mu$m. Tensile samples extracted from the thick plate under this condition are called the as-received and annealed (ARA) specimens. A series of low-temperature (25 °C to 250 °C) rolling-type TMT was applied to the ARA plates to a final thickness of 0.5 to 3 mm. The rolling reduction percentage or the true strain received during TMT varied from 90 to 98 pct or from 2.3 to 4.1, respectively. The trial TMT routes covered a wide range of processing conditions. Among them, an optimum TMT condition was determined. No static recrystallization heat treatment was carried out before tensile loading. Note that the strain level experienced during TMT in this study was around 2 to 4, which was smaller but comparable to the case of ECAE. Both processes could produce fine-grained materials. The material foundry can use a common rolling facility to produce large-scaled superplastic sheets for further forming. It does not need to redesign the extrusion or pressing machine. Also, the TMT prevents the troublesome water quenching after annealing, and it excludes the prolonged overaging heat treatment during TMT as used for other Al alloys.[2] Selected results from our parallel study on the LTSP 8090 Al-2.4wtpctLi-1.2wtpctCu-0.7wtpctMg alloy are also included for comparison and confirmation.

Constant crosshead speed tensile tests were conducted using an Instron (Massachusetts, USA) 5582 universal testing machine equipped with a three-zone furnace, with the loading direction parallel to the rolling direction. A heating rate of 5°/min was determined to produce optimum LTSP elongation performance and instrument stability without thermal fluctuations. The specimen gage length and width were 8 and 6 mm, respectively, with a shoulder radius of curvature of 2 mm. Step and jump strain rate tests[2] were conducted to determine the variation of strain-rate sensitivity as a function of strain rate and strain, respectively. The strain-rate difference be-tween the base and the jump (or step) was small (25 pct). To examine the operation of GBS, a two-step tensile test was performed. The specimens were first pulled to a certain level of strain, *e.g.*, $\varepsilon = 0.37$ or 1.21, then unloaded and cooled to room temperature. Surface polishing and line marking were done using 1-$\mu$m diamond pastes on a lens tissue wetted with acetone,[2] followed by continuous tensile reloading to an additional elongation of ~30 pct. The offsets or rotation of the marker lines were recorded by scanning electron microscopy (SEM). Microstructure and texture characterizations were performed using transmission electron microscopy (TEM) and electron backscattered diffraction (EBSD), as described elsewhere.[36,37]

In order to estimate the grain size dependence during LTSP, various grain sizes in the TMT processed specimens were produced. First, the TMT processed specimens were heated to 250 °C and held for 0 to 60 minutes (resulting in different grain sizes), followed by tensile loading at 250 °C and $1 \times 10^{-3}$ $s^{-1}$. Second, another group of the same TMT processed specimens were heated to 250 °C to 300 °C and held for 1 to 3 hours, then cooled to room temperature. After annealing, the specimens were reheated to 250 °C and tensile loaded at $1 \times 10^{-3}$ $s^{-1}$.

## III. RESULTS

### A. *Tensile Test Results*

The TMT processed 5083 alloy revealed a LTSP elongation of 511 pct under the optimum loading condition of 230 °C and $2 \times 10^{-3}$ $s^{-1}$. The ultimate tensile stress (UTS) typically occurred at a true tensile strain of $\varepsilon = 0.4$. The mechanical data on tensile elongation and ultimate tensile stress obtained from the ARA and TMT specimens at $1 \times 10^{-3}$ $s^{-1}$ are compared in Figure 1, covering the LTSP (≤250 °C), MTSP (medium temperatures between 300 °C to 400 °C), and HTSP (high temperatures ≥450 °C) regimes. In Figure 1(a), there are two maximum peaks, one of LTSP at ~230 °C and the other of HTSP at ~550 °C. Although the

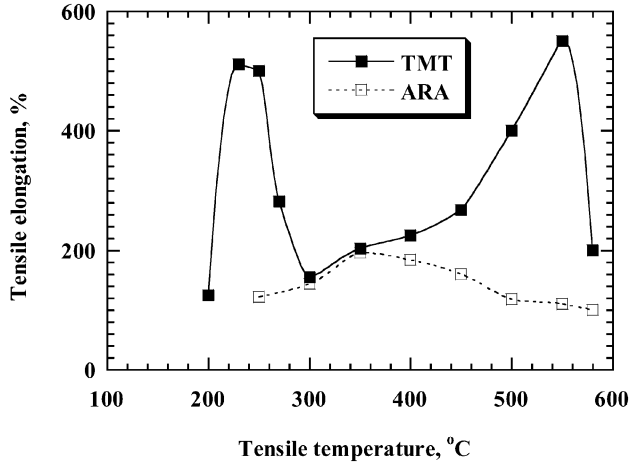


(*a*)

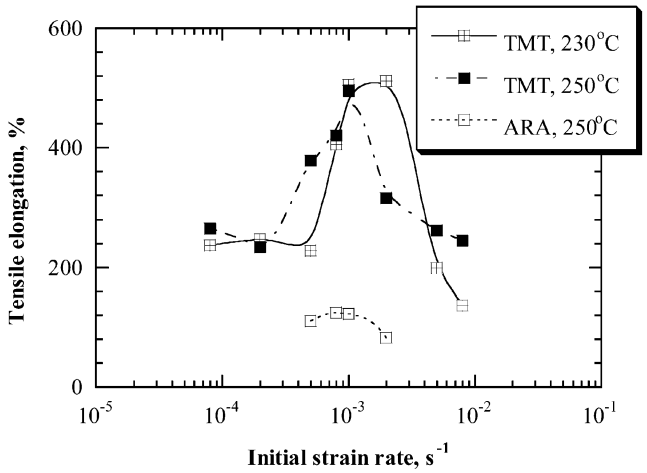


(*b*)

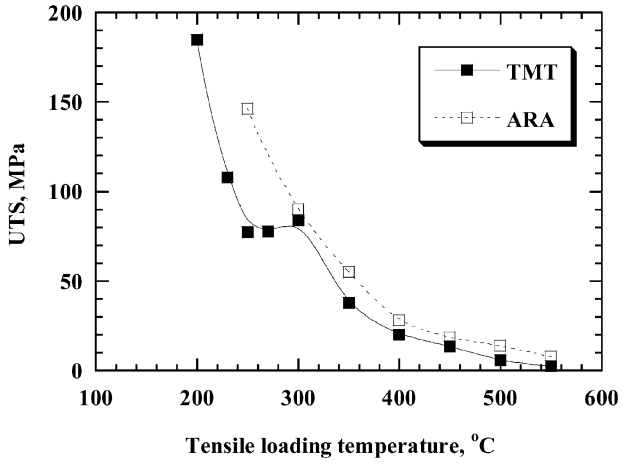


(*c*)

Fig. 1—Comparison of the tensile elongation as a function of (*a*) loading temperature (at $1 \times 10^{-3}$ s$^{-1}$) and (*b*) strain rate for the fine-grained TMT and coarse-grained ARA 5083 Al. (*c*) comparison for the ultimate tensile stress at $1 \times 10^{-3}$ s$^{-1}$.

values of tensile elongation were similar to each other (both ~450 to 550 pct), the controlling deformation mechanisms at these two temperatures are not the same. At low temperatures over 200 °C to 300 °C, the ultimate tensile stresses of the

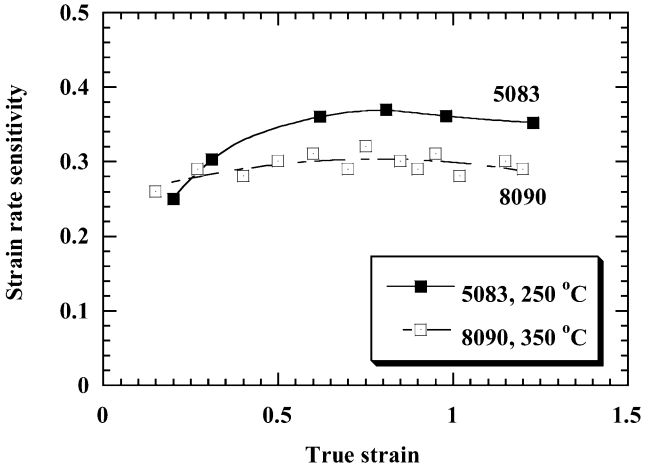


(*a*)

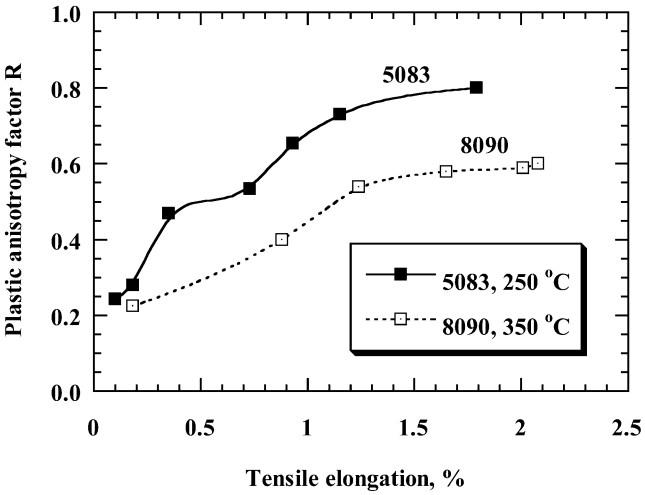


(*b*)

Fig. 2—Variation as a function of true strain for (*a*) strain-rate sensitivity obtained from the jump strain-rate test under the optimum strain rate condition of 1 to $2 \times 10^{-3}$ s$^{-1}$ and (*b*) plastic anisotropy factor for the fine-grained TMT 5083 and 8090 Al.

TMT specimens in Figure 1(c) were lower than the ARA ones by 50 to 80 MPa. For example, the UTS at 250 °C and $1 \times 10^{-3}$ s$^{-1}$ dropped from 146 MPa for the ARA materials to 77 MPa for the TMT processed ones, suggesting the stress reduction effect in the fine-grained thin sheets originated from the activation of GBS at low temperatures. This also implies that the controlling deformation mechanism in the ARA and TMT specimens should be different. But with increasing loading temperature over 300 °C to 400 °C, the mechanical results of the ARA and TMT groups gradually merged to similar regions, implying that the deformation mechanisms might be similar in this temperature range.

Figure 2 shows the variation of $m$ and plastic anisotropy factor $R$ ($= R_W/R_T$, where $R_W = (W_f - W_0)/W_0$ and $R_T = (T_f - T_0)/T_0$, and $W_f$, $W_0$, $T_f$, and $T_0$ are the final and initial tensile sample width and thickness, respectively) as a function of LTSP strain. Both $m$ and $R$ show an increasing trend with increasing LTSP strain until a saturated level. A value of $R \sim 0.8$ means that the material has plastically deformed in an isotropic manner. Data on the LTSP 8090 alloy are also included for comparison. Note that the optimum LTSP

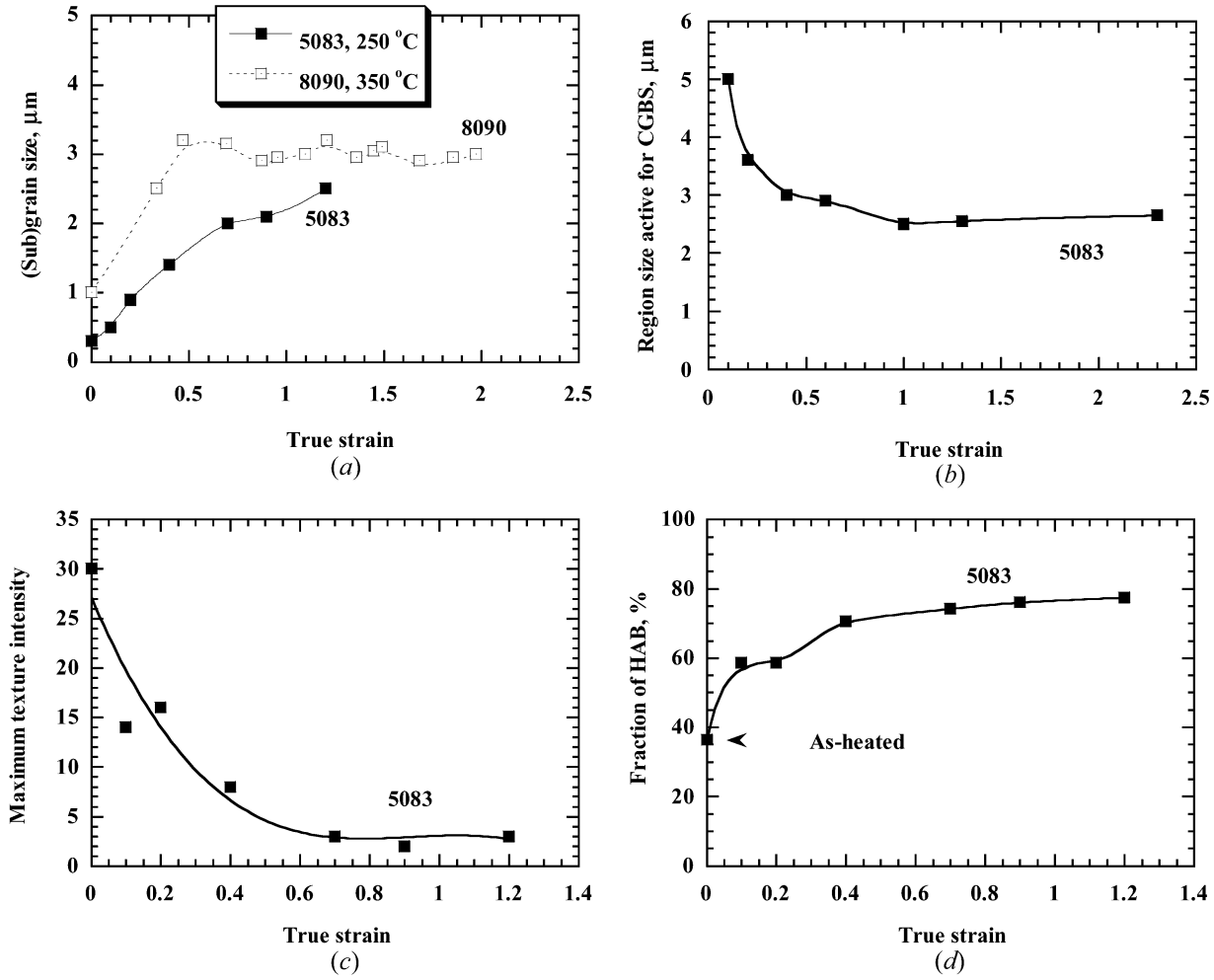


Fig. 3—Variation as a function of true strain for (*a*) grain size, (*b*) region size actually active for CGBS or GBS, (*c*) maximum texture intensity in pole figures, and (*d*) fraction of high-angle grain boundary with mutual misorientation angle >30 deg in the fine-grained TMT 5083 at 250 °C or 8090 Al at 350 °C.

temperature for 8090 Al was 100 °C higher than 5083 Al due to the presence of shearable $\delta'$ ($Al_3Li$) precipitates in 8090 Al up to ~330 °C.

### B. *Microstructure and Texture Evolution*

Systematic characterizations of microstructure, texture, and grain boundary mutual misorientation angles have been completed.[36,37] Figure 3 presents the variation of grain size *d*, larger region size *d′*[37] that cooperative grain boundary sliding (CGBS) actually proceeded (determined from the EBSD mapping), maximum texture intensity I in pole figures, and fraction of high-angle grain boundary (HAB with misorientation angle $\theta > 30$ deg) as a function of the LTSP strain. From Figure 3(a), it can be seen that the grain size remained $<3$ $\mu$m throughout the LTSP straining.

With the similar grain size over the LTSP straining, the grain boundary property and mutual grain misorientation have significantly evolved. With increasing strain, the region size that CGBS operates along the boundaries continued decreasing,[37] indicating that the individual GBS was not overwhelming during the initial stage and overall GBS would finally take over the deformation at a later straining stage of $\varepsilon \geq 1.0$. This effect can also be realized from Figures 3(c) and (d), where the strong texture gradually decreased and the HAB fraction gradually increased with increasing strain due to the gradual operation of GBS along most HAB. The previous results suggest that the controlling deformation mechanism might vary gradually as a function of LTSP strain. Discrepancy in the early reported parameters characterizing the controlling deformation mechanism might be related to the different straining stages under consideration.

### C. *Surface Marking Offset*

For fine-grained materials, it is always interesting to ask whether GBS would still operate smoothly at low temperatures at, for example, $0.6T_m$ or even $0.4T_m$. What would be the lowest temperature for GBS? The answer would be affected by the grain size and grain boundary character. For the current study, the initial grain size before LTSP straining was ~0.5 to 1.0 $\mu$m, and the initial HAB fraction was ~40 pct. The following equations have been proposed by Langdon,[41]

$$\varepsilon_{GBS} = \psi \frac{\overline{U}_t}{d_{eff}} \qquad [1]$$

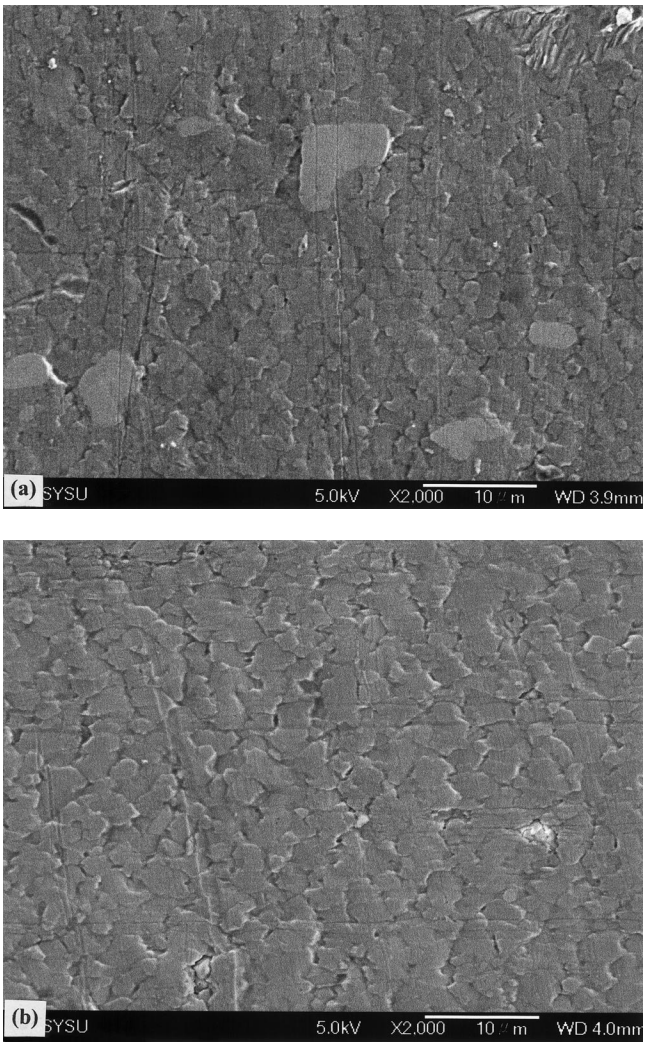


Fig. 4—SEM micrographs showing the offsets of surface marker lines in the TMT 5083 specimens loaded at 250 °C and $1 \times 10^{-3}$ s$^{-1}$ (*a*) $\varepsilon \sim 0.4$ and (*b*) $\varepsilon \sim 1.2$. The loading direction is nearly horizontal.

and

$$R_{\text{GBS}} = \frac{\varepsilon_{\text{GBS}}}{\varepsilon_{\text{reload}}} \qquad [2]$$

where $\varepsilon_{\text{GBS}}$ is the strain contributed by GBS, $\psi$ a coefficient taken for 0.8 for transverse marker lines,[42] $\overline{U}_t$ the average offsets parallel to the stress axis, $d_{\text{eff}}$ the mean linear intercept grain size actually undergoing CGBS or GBS, $R_{\text{GBS}}$ the contribution of GBS, and $\varepsilon_{\text{reload}}$ the relative strain for the reloading after polishing and marking. The average offset $\overline{U}_t$, was estimated for about 150 grain boundaries.

For the initial straining stage, the LTSP 5083 specimen was first pulled at 250 °C and $1 \times 10^{-3}$ s$^{-1}$ to 45 pct ($\varepsilon_{\text{l}} = 0.37$), followed by surface marking and reloading to a total elongation of 70 pct ($\varepsilon_{\text{t}} = 0.53$, or $\varepsilon_{\text{reload}} = 0.16$). Grain boundary sliding could be observed by some small offsets of marker lines with few large steps on the surface, as shown in Figure 4(a). Since the material at this initial straining stage contained many subgrains, on which performing GBS was difficult, the large offset steps are referred to the HAB that proceeded CGBS. It seems that GBS along individual grains was not significant during the initial straining. The estimated $d_{\text{eff}}$ was about 2 times of the linear intercept grain size, or ~3.0 $\mu$m, and the average $\overline{U}_t$ was ~0.162 $\mu$m. According to Eqs. [1] and [2], the contribution of GBS, $R_{\text{GBS}}$, was ~27 pct.

Another LTSP 5083 specimen was strained at 250 °C and $1 \times 10^{-3}$ s$^{-1}$ to 235 pct ($\varepsilon_{\text{l}} = 1.21$), followed by marking and reloading to a total elongation of 285 pct ($\varepsilon_{\text{t}} = 1.35$, or $\varepsilon_{\text{reload}} = 0.14$). The GBS along individual grains became more significant, as shown in Figure 4(b). The marker lines showed limited or substantial offsets while crossing almost all grain boundaries, and the grains continuously remained equiaxed in shape until failure. The mean $d_{\text{eff}}$ was determined to be nearly equal to the linear intercept grain size, or ~2.65 $\mu$m, and the average $\overline{U}_t$ was measured to ~0.288 $\mu$m; thus, the contribution of GBS was ~62 pct.

It seems assured that GBS did operate at temperatures as low as 200 °C ($0.5T_m$) for the current fine-grained Al alloys, especially for the later straining stage. For some even finer grain sizes in alloys processed by forging or ECAE, the grain size can be reduced to 0.1 to 0.3 $\mu$m[29–33] and GBS might be able to proceed at $0.4T_m$. For instance, the Zn-Al alloy processed by TMT or ECAE could show LTSP and GBS near room temperature (~25 °C to 100 °C or 0.40 to $0.50T_m$).[29,30] Below $0.4T_m$, thermal activated dislocation flow[43] would control the deformation. Furthermore, for pure element materials with little impurities fabricated by electrodeposition,[35] GBS might extend its operation at even $0.2T_m$.

## IV. ANALYSES OF DEFORMATION MECHANISMS

For fine-grained Al-Mg alloys deformed at elevated temperatures, three possible mechanisms should be considered. First, the typical superplastic deformation controlled by GBS would exhibit an $m$ value around 0.5 ($n = 1/m = 2$) and have a strong grain size dependency;[44] *i.e.*,

$$\dot{\varepsilon} = A \frac{E\mathbf{b}}{\mathrm{k}T} D_{\text{eff}} \left(\frac{\mathbf{b}}{d}\right)^p \left(\frac{\sigma - \sigma_{th}}{E}\right)^2 \qquad [3]$$

where $A$ is a coefficient related to grain boundary structure; k the Boltzmann's constant; $D_{\text{eff}}$ the effective diffusion coefficient, including lattice diffusion ($D_l$), grain boundary diffusion ($D_{gb}$), and dislocation core pipe diffusion ($D_p$); **b** the Burgers vector; $d$ the grain size; $p$ the grain size exponent close to 2 to 3; $\sigma_{th}$ the threshold stress; and $E$ the elastic modulus. The second acting mechanism might be the power-law dislocation creep with an average $m$ value around 0.2 and no grain size dependence;[45] *i.e.*,

$$\dot{\varepsilon} = B \frac{E\mathbf{b}}{\mathrm{k}T} D_{\text{eff}} \left(\frac{\sigma - \sigma_{th}}{E}\right)^5 \qquad [4]$$

where $B$ is another coefficient related to dislocation creep. Third, the solute drag creep for aluminum alloys with a sufficient amount of Mg should be active. The controlling rate equation[46] is

$$\dot{\varepsilon} = C \frac{\mathrm{k}T}{E} D_s \left(\frac{\sigma}{E}\right)^3 \qquad [5]$$

where $C$ is a constant and $D_s$ is the diffusion coefficient of the solute in the Al matrix.

From the tensile test data on the TMT specimens, it would

exhibit LTSP in the temperature ranges of 230 °C to 250 °C and HTSP at temperatures above 450 °C. At the medium temperatures between 300 °C and 400 °C, tensile elongation was decreased due to the occurrence of inhomogeneous partial recrystallization resulting in inhomogeneous microstructures. With increasing test temperature above 450 °C, complete recrystallization would lead to an equiaxed and homogeneous grain structure. On the basis of tensile test results and microstructural observations, deformation mechanisms will be examined in three temperature ranges, namely, 200 °C to 250 °C, 300 °C to 400 °C, and 450 °C to 550 °C. Also the deformation mechanisms of the ARA specimens will also be discussed.

### A. *Deformation Mechanisms at 200 °C to 250 °C*

#### 1. *Apparent strain rate sensitivity ($m_a$) and activation energy ($Q_a$)*

The engineering stress and strain curves were transformed into true stress-strain curves, assuming uniform thinning. This assumption was checked by interrupting tensile loading and measuring the specimen dimension at selected strain levels, such as $\varepsilon = 0.2, 0.6, 1.0, 1.5$, *etc*. It was found that when $\varepsilon < 1.0$ the straining was fairly uniform and the true stress could be directly transferred with high accuracy. Thus, in this study, the analysis was made at two strains, one at the initial stage of $\varepsilon = 0.4$ and the other at a later stage of $\varepsilon = 1.0$. Figure 5(a) shows the apparent strain-rate sensitivity $m_a$ for 200 °C to 250 °C at $\varepsilon = 0.4$. The average $m_a$ values at $\varepsilon = 0.4$ and 1.0 over this temperature range were ~0.25 and ~0.31, as listed in Table II. The apparent activation energy was extracted either from $\ln \dot{\varepsilon}$ *vs* $1000/\mathrm{R}T$ under a constant stress condition, or $\ln \sigma$ *vs* $1000/n\mathrm{R}T$ under a constant strain rate condition. The $Q_a$ calculated by these two methods was approximately 120 kJ/mole at $\varepsilon = 0.4$ (Figure 5(b)) and $\varepsilon = 1.0$.

#### 2. *Threshold stress ($\sigma_{th}$) and true strain rate sensitivity ($m_t$)*

There might exist a threshold stress $\sigma_{th}$, below which a negligible deformation rate can be detected.[47,48] The threshold stress could be appreciably high at low deformation temperatures and decreases gradually with increasing temperature.[49] The value of $\sigma_{th}$ was determined using a linear extrapolation on a double-linear plot of $\dot{\varepsilon}^{1/n}$ against $\sigma$ for selected values of $n$ at each temperature. The fitted straight line intersects the stress axis at zero strain rate and gives the value of $\sigma_{th}$.

In the temperature range of 200 °C to 250 °C, numerous selections using $n = 2$, 2.5, 3, 3.5, and 4 were tried. Excluding the stress data on 200 °C at higher rates of $5 \times 10^{-3}$ and $1 \times 10^{-2}$ $s^{-1}$, since they seemed to lie outside the LTSP region, the most probable true stress exponent $n_t$ seemed to be 3.5 (or true strain rate sensitivity $m_t$ of ~0.3), which corresponded to higher correlation coefficients, as shown in Figure 5(c) for $\varepsilon = 0.4$. It is an $n$ value between those for power-law dislocation creep ($n_t \sim 5$, ranging within 4 to 8) and solute drag creep ($n_t = 3$). Both mechanisms might have been operating and competing during this initial stage, contributing the observed strain rate. The extracted $\sigma_{th}$ values for 200 °C, 230 °C, and 250 °C at $\varepsilon = 0.4$ were 67.92, 23.58, and 16.98 MPa, respectively. Park and Mohamed[50] have proposed the following relationship:

$$\frac{n_a}{n_t} = \frac{\sigma}{\sigma - \sigma_{th}} \qquad [6a]$$

or

$$\frac{m_t}{m_a} = \frac{\sigma}{\sigma - \sigma_{th}} \qquad [6b]$$

For example, the true stress is 135.08 MPa at 230 °C and $1 \times 10^{-3}$ $s^{-1}$, and the effective stress $\sigma - \sigma_{th}$ would be 111.5 MPa, so the value of $\sigma/(\sigma - \sigma_{th})$ is around 1.2, the same as $n_a/n_t$. Thus, the estimated value of true stress exponent should be reasonable. Parallel analysis was also done using the data on $\varepsilon = 1.0$, and $n_t$ was determined to be 2.8 (or $m_t \sim 0.35$).

#### 3. *True activation energy, $Q_t$*

Without accounting for the temperature-dependent elastic constant term $E(T)$, the true activation energy can be evaluated according to the equation of

$$Q_t = -\mathrm{R} \frac{\partial(\ln \dot{\varepsilon})}{\partial\left(\frac{1}{T}\right)}\Big|_{\sigma-\sigma_{th}} \qquad [7a]$$

and

$$Q_t = n\mathrm{R} \frac{\partial[\ln(\sigma - \sigma_{th})]}{\partial\left(\frac{1}{T}\right)}\Big|_{\dot{\varepsilon}} \qquad [7b]$$

Taking $(\sigma - \sigma_{th}) = 100$ MPa, the slope of the double linear plot of $\ln \dot{\varepsilon}$ against $1000/\mathrm{R}T$ based on Eq. [7a] was 73.0 kJ/mole. On the other hand, taking $m_t = 0.3$ and $\dot{\varepsilon} = 1 \times 10^{-3}$ $s^{-1}$, the estimated activation energy under constant strain rate based on Eq. [7b] was 72.5 kJ/mole (Figure 5(d)). If the temperature dependence of elastic modulus is included, then selecting the constant normalized stress condition of $(\sigma - \sigma_{th})/E = 1.5 \times 10^{-3}$, $Q_t$ is ~70 kJ/mole, as compared in Table II. Parallel calculations on $\varepsilon = 1.0$ yielded a $Q_t$ of ~90 kJ/mole, also compiled in Table II.

Both of these two values of $Q_t$ were much lower than the Mg diffusion in Al matrix (136 kJ/mole) and self-diffusion of pure Al (142 kJ/mole), but close to the dislocation pipe diffusion in Al (82 kJ/mole) and grain boundary diffusion in Al (84 kJ/mole).[51] Although the activation energy of pipe diffusion or grain boundary diffusion of Mg atom in Al was not reported, it is postulated to be similar to or slightly lower than the diffusion cases for Al, judging from the relative $Q$ for Mg and Al lattice diffusion. Therefore, on the basis of the estimated true activation energy in the temperature range of 200 °C to 250 °C, the rate-controlling diffusion step might be dislocation pipe diffusion or grain boundary diffusion for Al or Mg atoms in the Al matrix.

For confirmation, parallel analyses on the 8090 alloy under the LTSP regime were done. The results at $\varepsilon = 0.5$ give values of $Q_a \sim 92$ kJ/mole, $n_t \sim 3.0$ (or $m_t \sim 0.33$), and $Q_t \sim 80$ kJ/mole, in good agreement with those obtained from the 5083 LTSP alloys.

#### 4. *Grain size exponent, p*

If grain boundary sliding were dominant, the $p$ value in Eq. [3] would be 2 for lattice or pipe diffusion controlled

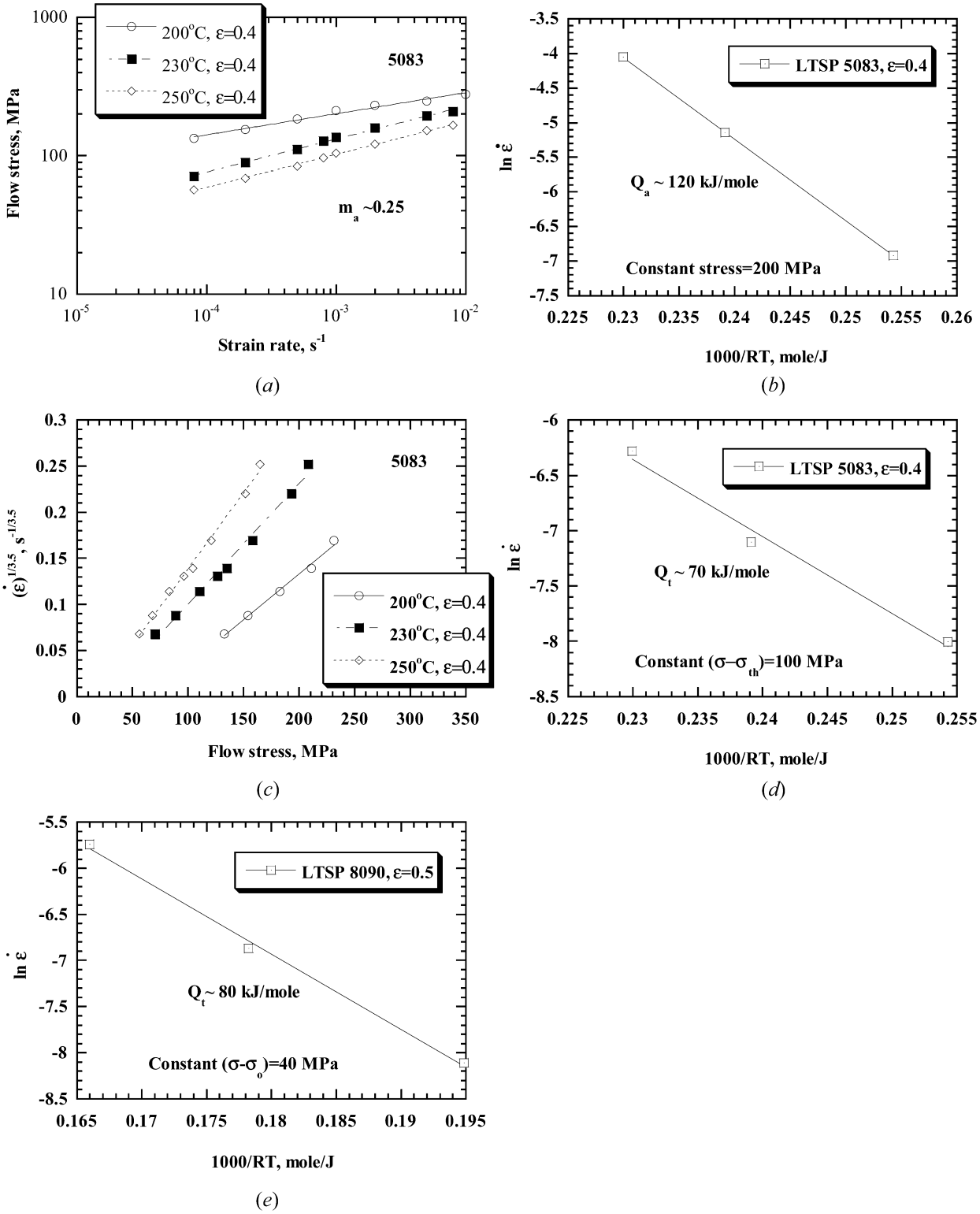


Fig. 5—The analyses on the LTSP 5083 Al for extractions of (*a*) apparent strain-rate sensitivity $m_a$, (*b*) apparent activation energy $Q_a$ (*c*) threshold stress, and (*d*) true activation energy $Q_t$. (*e*) true activation energy $Q_t$ for the LTSP 8090 Al.

or 3 for grain boundary diffusion governed. If the power-law dislocation creep or solute drag creep were dominant, the *p* value in Eqs. [4] and [5] would be zero. For discussion of the relationship between grain size and flow stress, Eq. [3] can be rewritten as

$$\dot{\varepsilon} = A' \left(\frac{\mathbf{b}}{d}\right)^p \left(\frac{\sigma - \sigma_o}{E}\right)^n \exp\left(-\frac{Q}{RT}\right) \qquad [8]$$

where $A'$ is a coefficient. At constant temperature, Eq. [8] can be written as

**Table II. Summary of the Extracted Parameters and the Proposed Deformation Mechanisms and Rate Controlling Diffusion Paths for the TMT Fine-Grained and ARA Coarse-Grained 5083 Al**

| | TMT Specimens | | | | ARA Specimens | |
|---|---|---|---|---|---|---|
| | Low Temperature (200 °C to 250 °C) | | Medium Temperature (300 °C to 400 °C) | High Temperature (450 °C to 550 °C) | Low Temperature (200 °C to 250 °C) | High Temperature (450 °C to 550 °C) |
| True strain $\varepsilon$ | 0.4 | 1.0 | 0.4 | 0.4 | 0.3 | 0.3 |
| $m_a$ | ~0.25 | ~0.31 | ~0.26 | ~0.43 | ~0.14 | ~0.3 |
| $Q_a$, kJ/mole | ~120 | ~120 | ~153 | 158 | — | ~160 |
| $m_t$ | ~0.30 | ~0.35 | ~0.33 | ~0.55 | ~0.2 | ~0.33 |
| $Q_t$, kJ/mole | ~70 | ~90 | ~76 | ~82 | — | 147 |
| $p$ | ~0 | ~1.1 | ~0.3 | ~2.0 | ~0.6 | — |
| Deformation mechanisms | major: solute drag creep minor: power-law creep + grain boundary sliding | major: grain boundary sliding minor: solute drag creep | major: solute drag creep minor: grain boundary sliding | major: grain boundary sliding minor: solute drag creep | power-law dislocation creep | solute drag creep |
| Rate-controlling diffusion path | pipe diffusion of Mg atom in Al | grain boundary diffusion of Al | pipe diffusion of Mg atom in Al | grain boundary diffusion of Al | — | pipe diffusion of Mg atom in Al |




Fig. 6—Variation of ln $(\sigma/E)^n$ *vs* ln $(1/d)$ for the LTSP 5083 Al (loaded at 250 °C and $1 \times 10^{-3}$ s$^{-1}$) and 8090 Al (loaded at 350 °C and $8 \times 10^{-4}$ s$^{-1}$); from the slope, the grain size exponent $p$ can be evaluated. The 5083 (1) data are referred to the group of specimens that were first annealed at 250 °C for 0 to 60 min, and the 5083 (2) ones are referred to the other group that were annealed at 250 °C to 300 °C for 1 to 3 h before tensile loading.

$$\ln \dot{\varepsilon} = \ln B' + p \ln\left(\frac{\mathbf{b}}{d}\right) + n \ln\left(\frac{\sigma - \sigma_o}{E}\right) \qquad [9]$$

where $B'$ is a temperature-dependent coefficient. Determination of $p$ could be done by (a) finding the relationship between $\sigma$ and $d$ under the constant strain rate condition or (b) determining the dependence between $\dot{\varepsilon}$ and $d$ at any given $\sigma$ value. In this study, the various grain size data in specimens subjected to different periods of static annealing time of 0 to 60 minutes at 250 °C were obtained (varying within 0.5 to 3 $\mu$m). The same group of specimens was tensile loaded at 250 °C and $1 \times 10^{-3}$ s$^{-1}$, and the stresses were recorded. Thus, the first method can be applied to determine $p$. The double linear plot of ln $(\sigma - \sigma_o/E)^n$ against ln $(1/d)$ is presented in Figure 6. The slope of this plot or $p$ was around zero for the LTSP 5083 Al at $\varepsilon = 0.4$, which means that, during the initial straining, there was no dependence between strain rate and grain size.

For confirmation of the $p$ value over a wider range of $d$, another set of tensile loading was performed on the 5083 TMT specimens annealed at higher temperatures for 1 to 3 hours. Static annealing at $T > 250$ °C for a long time will result in much larger uneven grain sizes ranging from 3 to 15 $\mu$m. Also, the ARA specimen, with a grain size of 25.2 $\mu$m, was included. As presented in Figure 6, the estimated $p$ value when loaded at 250 °C to $\varepsilon = 0.4$ over a wide range of $d$ from 1.75 to 25.2 $\mu$m was still low (~0.6). It is assured that, during the initial LTSP straining stage, there was little grain size dependence.

Based on the preceding determination and discussion, with $m \sim 0.3$, $Q \sim 70$ kJ/mole, and $p \sim 0$ at $\varepsilon = 0.4$, the most important deformation mechanism during the initial LTSP straining in 5083 Al seems to be solute drag creep ($m \sim 0.33$), followed by minor contribution from power-law dislocation creep ($m \sim 0.2$). Grain boundary sliding seemed to play a less governing role over this stage. Since solute drag creep may contribute most, the rate-controlling diffusion step

may be dislocation pipe diffusion of the Mg atom in the Al matrix, as summarized in Table II.

When the LTSP 5083 specimens were strained to $\varepsilon = 1.0$, $p$ increased from ~0 at $\varepsilon = 0.4$ to a value ~1.1, as shown in Figure 6. It is postulated that $p$ would increase to 2 or above at $\varepsilon$ greater than 1.5 (or tensile elongation greater than 300 pct). It suggests that grain boundary sliding has gradually increased its contribution at larger strains. This result is consistent with the TEM and EBSD observations,[37] *i.e.*, increasing fraction of high-angle grain boundaries and decreasing intensity of maximum texture contours with increasing LTSP straining.

Similar determinations of the $p$ values in the LTSP 8090 Al alloys were also completed, as also shown in Figure 6. It was found that $p$ was ~1.0 at 350 °C and $\varepsilon \sim 0.5$. It seems that the grain boundary evolution proceeded faster in the LTSP 8090 (at 350 °C) than in the LTSP 5083 (at 250 °C), since $p$ reaches 1.0 at $\varepsilon = 0.5$ for 8090 Al but at $\varepsilon = 1.0$ for 5083 Al. This effect should result from the higher loading temperature for the 8090 Al alloy.

5. *Deformation mechanisms at 230 °C to 250 °C*

In analyzing the LTSP data, those obtained at 200 °C sometimes behaved slightly differently from the cases of 230 °C and 250 °C. The tensile elongations at 200 °C were also apparently lower than those at the other two temperatures. Therefore, separate confirmation using only the data on 230 °C and 250 °C at $\varepsilon = 0.4$ was undertaken. Taking $\sigma = 200$ MPa or $\dot{\varepsilon} = 1 \times 10^{-3}$ s$^{-1}$, with $m_a = 0.26$, the estimated $Q_a$ was around 118 kJ/mole. In the same way described previously, the best fitted $m_t$ value in the temperature range of 230 °C to 250 °C was also 0.3. The estimated activation energy under constant effective stress or strain rate was 89.5 or 92.9 kJ/mole. Considering the temperature dependence of elastic modulus, the extracted true activation energy was 84.7 or 88.2 kJ/mole. According to this confirmation result, the true activation energy of ~86 kJ/mole is very close to dislocation pipe diffusion of Mg or Al atoms in the Al matrix. Thus, the above interpretations should be highly reliable.

## B. *Deformation Mechanism at 300 °C to 400 °C*

In the temperature range of 300 °C to 400 °C, it exhibited lower ductility than the LTSP and HTSP regimes. It seems that this temperature range was in the transition area between LTSP and HTSP. The grain structure evolved upon heating and held at 300 °C to 400 °C was not uniform, with a mixture of partially and fully recrystallized microstructures. Determining the deformation mechanisms at this MTSP range would be helpful in understanding the difference between LTSP and HTSP.

Due to the limited tensile elongation, only data on $\varepsilon = 0.4$ were analyzed. The relationship between flow stress and strain rate at 300 °C, 350 °C, and 400 °C is depicted in Figure 7(a). The $m_a$ values for three temperatures were ~0.22, 0.28, and 0.30, with an average $m_a$ of 0.26. Selecting $\sigma = 40$ MPa under the constant stress condition, or $\dot{\varepsilon} = 1 \times 10^{-3}$ s$^{-1}$ for the constant strain rate condition, the extracted $Q_a$ was ~156.8 and 150.0 kJ/mole, respectively, as shown in Figure 7(b).

In the temperature range of 300 °C to 400 °C, the most probable $n_t$ seemed to be 3 with a higher correlation coefficient, as shown in Figure 7(c). It is an $n$ value characteristic of solute drag creep. The extracted $\sigma_{th}$ values of 300 °C to 400 °C were 28.00, 7.92, and 2.11 MPa, respectively. It was noted that the flow stresses, as well as $\sigma_{th}$, at 300 °C were all higher than those at 230 °C and 250 °C (*cf.* Figure 1(c)), presumably due to the larger and uneven grain size at 300 °C, which suppressed the smooth operation of GBS. Considering threshold stress, the estimated activation energy was 79.2 or 81.3 kJ/mole, as shown in Figure 7(d). Including the temperature dependence of elastic modulus, $Q_t$ was around 74.1 kJ/mole under the constant normalized stress condition and around 76.9 kJ/mole under the constant strain rate condition.

The average true activation energy estimated above is around 76 kJ/mole, and the $m_t$ value is 0.33. It appears that the dominant deformation mechanism should be solute drag creep at 300 °C to 400 °C, and the rate-controlling diffusion step might be dislocation pipe diffusion of Mg atom in the Al matrix, as compared in Table II. It was difficult to determine the $p$ value precisely in this temperature range, because the systematic tensile tests at 300 °C to 400 °C on the specimens with different grain sizes were not carried out. Also, the grain size was not uniform, with $d \sim 3$ $\mu$m for the partially recrystallized regions and $d \sim 15$ $\mu$m for the fully recrystallized ones. Calculation of the $p$ value was attempted from the specimens of ARA and TMT, with different average grain sizes of ~25.0 and ~6.0 $\mu$m, respectively. The tensile true stresses at $\varepsilon = 0.4$ of these two specimens were 97.5 and 82.6 MPa at 300 °C and $1 \times 10^{-3}$ s$^{-1}$. The estimated $p$ value was still as low as ~0.3, basically with nil dependence between grain size and true stress at 300 °C. This is in agreement with the prediction of Eq. [5] that there is no grain size dependence if solute drag creep dominates. Meanwhile, the specimens with distinctly different grain sizes of 25 and 6 $\mu$m all exhibited similar tensile elongations of ~200 pct, which is also the among the elongation levels expected for typical solute drag creep at intermediate temperature ranges.

## C. *Deformation Mechanisms at 450 °C to 550 °C*

The apparent strain-rate sensitivity $m_a$ of the TMT 5083 Al in the HTSP temperature range of 450 °C to 550 °C is shown in Figure 8(a), being 0.38, 0.39, and 0.50 at 450 °C, 500 °C, and 550 °C, respectively. The $Q_a$ at $\sigma = 10$ MPa or $\dot{\varepsilon} = 1 \times 10^{-3}$ s$^{-1}$ was estimated to be 159.5 or 156.0 kJ/mole (Figure 8(b)). In this temperature range, the most probable $n_t$ was found to be 1.8, as shown in Figure 8(c). And the estimated values of $\sigma_{th}$ at 450 °C, 500 °C, and 550 °C were 4.49, 1.85, and 0.39 MPa, respectively. Figure 8(d) shows the extraction of activation energy to be 82.2 or 90.1 kJ/mole by the two methods. With $E(T)$ considerations, $Q_t$ became 77.5 and 85.5 kJ/mole (or an average of ~82 kJ/mole), consistent with grain boundary diffusion of Al.

The stress levels for the ARA 5083 specimens were typically 2 times those of the TMT ones at high temperatures. Since they do not seem to deform under the same deformation mechanism, one primarily by solute drag and the other mainly by GBS, it is inappropriate to evaluate the $p$ value by these two specimens. Parallel analyses on the HTSP 8090 Al over 500 °C to 550 °C yielded $p \sim 2$. On the basis of the preceding analyses and microstructure observations, the dominant deformation mechanism for the TMT-processed HTSP alloys is undoubtedly grain boundary sliding, and

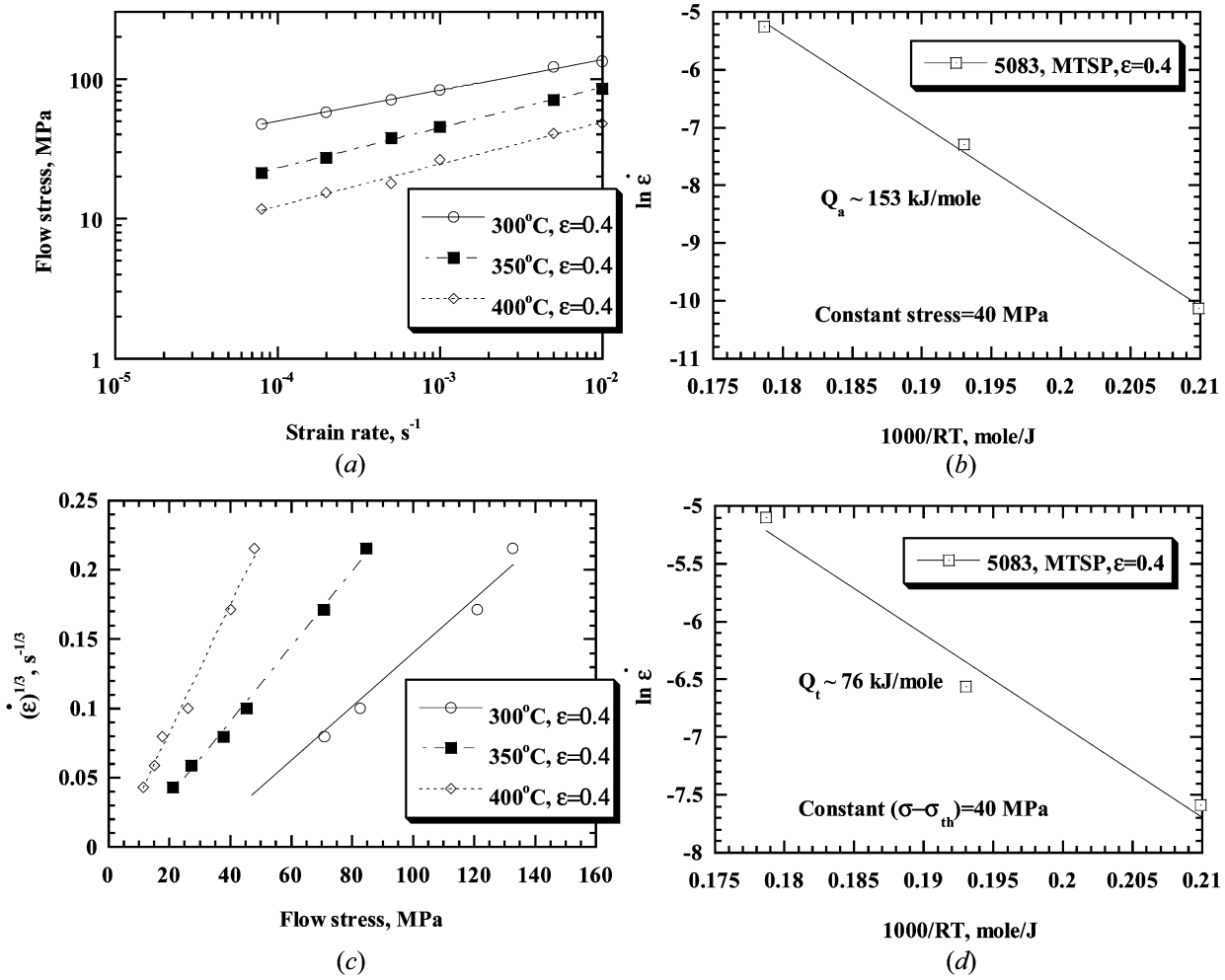


Fig. 7—The analyses on the MTSP 5083 Al for extractions of (*a*) apparent strain-rate sensitivity $m_a$ (*b*) apparent activation energy $Q_a$, (*c*) threshold stress, and (*d*) true activation energy $Q_t$.

the rate-controlling diffusion step should be grain boundary diffusion, as compared in Table II.

### D. *Deformation Mechanisms of ARA Specimens*

Similar analyses were also performed on the data obtained from the course-grained ARA specimens. The $m_a$ was ~0.14 at 250 °C and ~0.3 at a high temperature of ~550 °C. The true rate sensitivity $m_t$ extracted was 0.2 at 250 °C and 0.33 at high temperatures. The activation energy was determined to be around 147.4 kJ/mole over 450 °C to 550 °C. It seems that the deformation mechanisms of the ARA samples were power-law dislocation creep ($n \sim 5$) at low temperatures and solute drag creep ($n \sim 3$) at high temperatures. The rate-controlling diffusion step at high temperatures would be lattice diffusion of Al or Mg diffusion in the Al matrix (both with $Q \sim 130$ to 140 kJ/mole).

### E. *Comparison for Different Diffusion Paths*

The controlling diffusion path during deformation at low, medium, and high temperatures can also be judged from the overall effective diffusion coefficient $D_{\text{eff}}$, contributed by lattice diffusion coefficient $D_l$, grain boundary diffusion coefficient $D_{gb}$, and pipe diffusion coefficient $D_p$.

$$D_{\text{eff}} = D_l + \frac{\pi\delta}{d_{\text{eff}}} D_{gb} \quad [10]$$

and

$$D_{\text{eff}} = D_l + f_p D_p \quad [11]$$

where $D_l = 1.7 \times 10^{-4} \exp(-142{,}000/RT)$ m$^2$/s, $\delta D_{gb} = 5 \times 10^{-14} \exp(-84{,}000/RT)$ m$^2$/s with $\delta = 2b = 0.5726$ nm, and $f_p D_p = 1.7 \times 10^{-8} \exp(-82{,}000/RT)$ m$^2$/s.[51] Table III lists the relative values at 250 °C (LTSP), 350 °C (MTSP), and 500 °C (HTSP) for Al alloys. For LTSP and MTSP, pipe or grain boundary diffusion overwhelms lattice diffusion, consistent with the extracted $Q_t$ values that match closely with the pipe or grain boundary diffusion. For HTSP, these three diffusion paths provide compatible rates depending on the grain size, and the extracted $Q_t$ seems to correspond to grain boundary diffusion for the TMT specimens ($d \sim 8$ $\mu$m) but to lattice diffusion for the ARA samples ($d \sim 25$ $\mu$m).

## V. SUMMARY

The LTSP was observed in the 5083 Al-Mg base alloys after TMT. The maximum LTSP elongation was 511 pct, occurring at 230 °C and $2 \times 10^{-3}$ s$^{-1}$. The microstructure

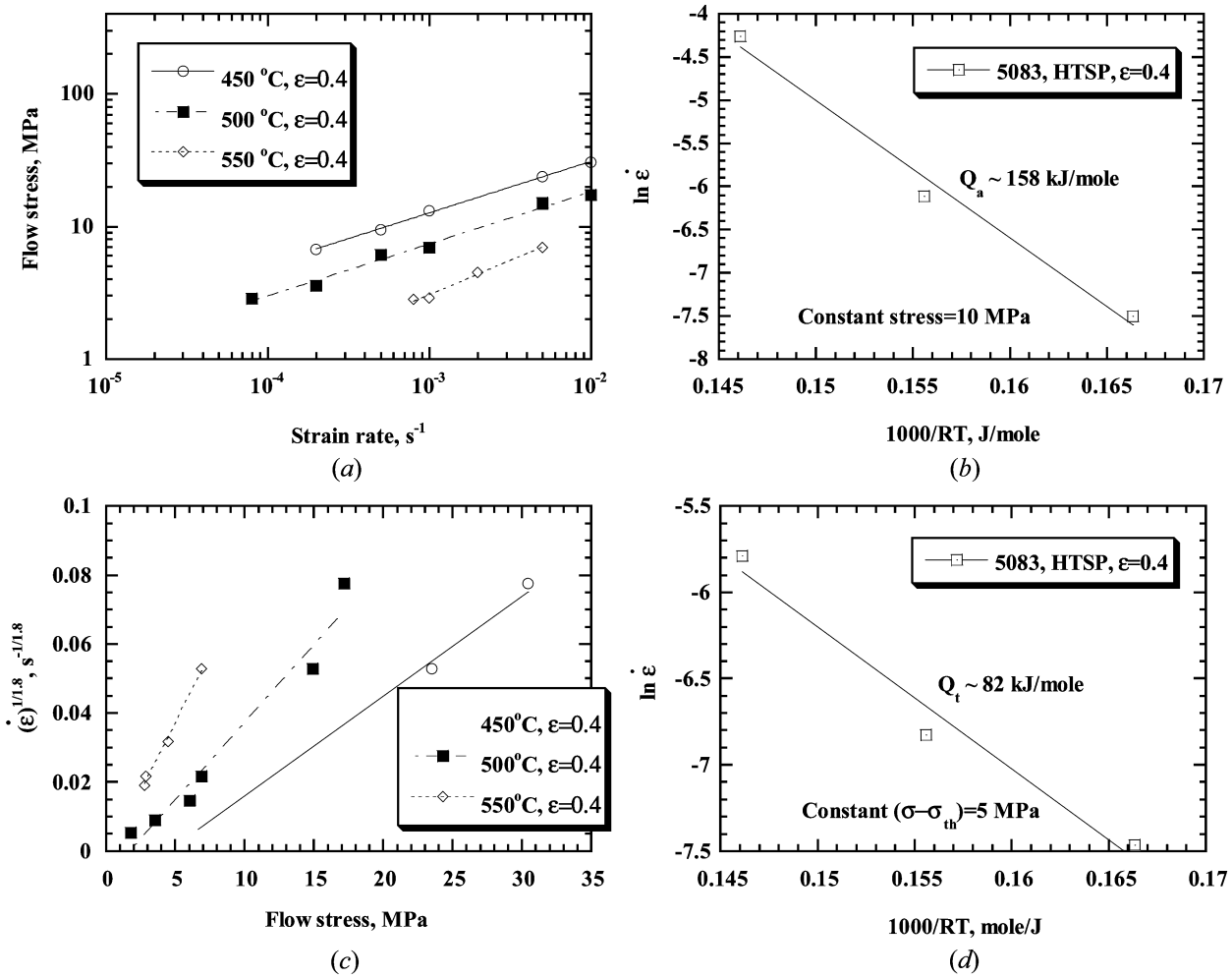


Fig. 8—The analyses on the HTSP 5083 Al for extractions of (*a*) apparent strain-rate sensitivity $m_a$, (*b*) apparent activation energy $Q_a$, (*c*) threshold stress, and (*d*) true activation energy $Q_t$.

**Table III. Comparison of the Relative Magnitudes of the Three Diffusion Paths: (1) Lattice, (2) Grain Boundary, and (3) Pipe Diffusion in the TMT and ARA Aluminum Specimens Loaded at 250 °C (LTSP), 350 °C (MTSP), and 500 °C (HTSP)**

| Specimen | $T$ (°C) | $d_{\text{eff}}$ ($\mu$m) | (1) $D_l$ (m$^2$/s) | (2) $\frac{\pi\delta}{d_{\text{eff}}} D_{gb}$ (m$^2$/s) | (3) $f_p D_p$ (m$^2$/s) | (2)/(1) | (3)/(1) |
|---|---|---|---|---|---|---|---|
| TMT | 250 | 3 | $1.1 \times 10^{-18}$ | $2.1 \times 10^{-16}$ | $1.1 \times 10^{-16}$ | 191 | 98 |
| | 350 | 6 | $2.1 \times 10^{-16}$ | $2.3 \times 10^{-15}$ | $2.3 \times 10^{-15}$ | 11 | 11 |
| | 500 | 8 | $4.2 \times 10^{-14}$ | $4.1 \times 10^{-14}$ | $4.8 \times 10^{-14}$ | 1.0 | 1.1 |
| ARA | 500 | 25 | $4.3 \times 10^{-14}$ | $1.3 \times 10^{-14}$ | $4.8 \times 10^{-14}$ | 0.3 | 1.1 |

evolution and deformation mechanisms were examined and discussed as a function of temperature and strain. The following conclusions can be drawn.

1. The fine-grained TMT 5083 specimens exhibited $m \sim 0.3$, 0.33, and 0.55 during the LTSP, MTSP, and HTSP. In contrast, the coarse-grained ARA 5083 alloy showed $m \sim 0.2$, 0.33, and 0.33 at the same temperature regimes.
2. Grain boundary sliding did occur in 5083 Al at temperatures as low as 200 °C ($0.5T_m$). It is expected that with further grain size refinement, GBS could extend its operation to $0.2T_m$.
3. With increasing LTSP straining from the initial ($\varepsilon \leq 0.5$) to later stages ($\varepsilon \geq 1.0$), the strain-rate sensitivity $m$ increased from 0.3 to 0.35, plastic anisotropy factor $R$ increased from 0.5 to >0.7, region size actually undergoing CGBS decreased from 5 to 2 $\mu$m, pole figure texture intensity decreased from 25 to <5, high-angle grain boundary fraction increased from 50 to 80 pct, grain size exponent $p$ increased from 0 to >1, and grain boundary sliding contribution increased from 27 to 62 pct. All of these observations indicate that the deformation mechanisms and their controlling diffusion paths varied with the evolution of grain and grain boundary structures.
4. During the initial LTSP stage ($\varepsilon \leq 0.5$) in the TMT 5083 Al, there was little grain size dependence with $p \sim 0$, and the primary deformation mechanisms were solute

drag creep plus minor power-law creep. The rate controlling diffusion path was dislocation pipe diffusion. At later stages ($\varepsilon \geq 1.0$), grain size dependence increased and grain boundary sliding gradually controlled the deformation. The rate controlling diffusion path became grain boundary diffusion.

5. During MTSP and HTSP in the TMT 5083 Al, solute drag creep and grain boundary sliding were the dominating deformation mechanisms, respectively.

## ACKNOWLEDGMENTS

The authors gratefully acknowledge the sponsorship from the National Science Council of the Republic of China under Project Nos. NSC 89-2216-E-110-014 and -041.

## REFERENCES

1. K. Higashi and M. Mabuchi: *Mater. Sci. Forum*, 1997, vols. 243–245, pp. 267-72.
2. H.P. Pu, F.C. Liu, and J.C. Huang: *Metall. Mater. Trans. A*, 1995, vol. 26A, pp. 1153-66.
3. R.Z. Valiev, D.A. Salimonenko, N.K. Tsenev, P.B. Berbon, and T.G. Langdon: *Scripta Mater.*, 1997, vol. 37, pp. 1945-50.
4. P.A. Friedman and A.K. Ghosh: *Metall. Mater. Trans. A*, 1996, vol. 27A, pp. 3827-39.
5. R. Verma, P.A. Friedman, A.K. Ghosh, S. Kim, and C. Kim: *Metall. Mater. Trans. A*, 1996, vol. 27A, pp. 1889-98.
6. M. Matsuo, T. Tagata, and N. Matsumoto: *Thermece'97*, T. Chandra and T. Sakai, eds., TMS, Warrendale, PA, 1997, pp. 1953-59.
7. Y. Wu, L.D. Castillo, and E.J. Lavernia: *Metall. Mater. Trans. A*, 1997, vol. 28A, pp. 1059-68.
8. S.N. Patankar and T.M. Jen: *Scripta Mater.*, 1998, vol. 38, pp. 1255-61.
9. T.R. McNelley, R. Crooks, P.N. Kalu, and S.A. Rogers: *Mater. Sci. Eng.*, 1993, vol. A166, pp. 135-43.
10. J. Wang, Z. Horita, M. Furukawa, M. Nemoto, N.K. Tsenev, R.Z. Valiev, Y. Ma, and T.G. Langdon: *J. Mater. Res.*, 1993, vol. 8, pp. 2810-16.
11. S.S. Woo, Y.R. Kim and D.H. Shin: *Scripta Mater.*, 1997, vol. 37, pp. 1351-58.
12. M. Kawazoe, T. Shibata, T. Mukai, and K. Higashi: *Scripta Mater.*, 1997, vol. 36, pp. 699-705.
13. T.G. Nieh, R. Kaibyshev, L.M. Hsiung, N. Nguyen, and J. Wadsworth: *Scripta Mater.*, 1997, vol. 36, pp. 1011–16.
14. E.M. Taleff, G.A. Henshall, T.G. Nieh, D.R. Lesuer, and J. Wadsworth: *Metall. Mater. Trans. A*, 1998, vol. 29A, pp. 1081-91.
15. R.Z. Valiev, D.A. Salimonenko, N.K. Tsenev, P.B. Berbon, and T.G. Langdon: *Scripta Mater.*, 1997, vol. 37, pp. 1945-50.
16. E.M. Taleff, G.A. Henshall, and J. Wadsworth: *Metall. Mater. Trans. A*, 1996, vol. 27A, pp. 343-52.
17. A.A. Tavassoli, S.E. Razavi, and N. Fallah: *Metall. Trans. A*, 1975, vol. 6A, pp. 591-94.
18. J.K. Kim and D.H. Shish: *Scripta Mater.*, 1998, vol. 38, pp. 991-98.
19. S.J. Hales, T.R. McNelley, and H.J. McQueen: *Metall. Trans. A*, 1991, vol. 22A, pp. 1037-47.
20. R.R. Sawtell and C.L. Jensen: *Metall. Trans. A*, 1990, vol. 21A, pp. 421-30.
21. T.G. Nieh, R. Kaibyshev, L.M. Hsiung, N. Nguyen, and J. Wadsworth: *Acta Mater.*, 1998, vol. 46, pp. 2789-2800.
22. T.R. McNelley, E.-W. Lee, and M.E. Mills: *Metall. Trans. A*, 1986, vol. 17A, pp. 1035-41.
23. R.Z. Valiev, A.V. Korznikov, and R.R. Mulyukov: *Mater. Sci. Eng.*, 1993, vol. A168, pp. 141-48.
24. H.P. Pu and J.C. Huang: *Scripta Metall. Mater.*, 1993, vol. 28, pp. 1125-30.
25. R.Z. Valiev: *Mater. Sci. Forum*, 1997, vol. 243-245, pp. 207-12.
26. I.C. Hsiao and J.C. Huang: *Scripta Mater.*, 1999, vol. 40, pp. 697-703; *Mater. Sci. Forum*, 1999, vols. 304–306, pp. 639-34.
27. M. Mabuchi, H. Iwasaki, K. Yanase, and K. Higashi: *Scripta Mater.*, 1997, vol. 36, pp. 681-86.
28. T. Mukai, T.G. Nieh, and K. Higashi: *Thermece'97*, T. Chandra and T. Sakai, eds., TMS, Warrendale, PA, 1997, pp. 1847-52.
29. T.K. Ha, W.B. Lee, C.G. Park, and Y.W. Chang: *Metall. Mater. Trans. A*, 1997, vol. 28A, pp. 1711-13.
30. M. Furukawa, Y. Ma, Z. Horita, M. Nemoto, R.Z. Valiev, and T.G. Langdon: *Mater. Sci. Eng.*, vol. A241, pp. 122-28.
31. A.V. Sergueeva, V.V. Stolyarov, R.Z. Valiev, and A.K. Mukherjee: *Scripta Mater.*, 2000, vol. 43, pp. 819-24.
32. R.M. Imayev, G.A. Salishecev, M.R. Shagiev, V.M. Imayev, N.K. Gabdullin, A.V. Kuznetsov, O.N. Senkov, and F.H. Froes: *Mater Sci. Forum*, 1999, vols. 304–306, pp. 195-200.
33. V.M. Imayev, G.A. Salishchev, M.R. Shagiev, A.V. Kuznetsov, R.M. Imayev, O.N. Senkov, and F. H. Froes: *Scripta Mater.*, 1999, vol. 40, pp. 183-290.
34. S.X. McFadden, R.S. Mishra, R.Z. Valiev, A.P. Zhilyaev, and A.K. Mukherjee: *Nature*, 1999, vol. 398, pp. 684-86.
35. L. Lu, M. L. Sui, and K. Lu: *Science*, 2000, vol. 287, pp. 1463-66.
36. I.C. Hsiao, J.C. Huang, and S.W. Su: *Mater. Trans. JIM*, 1999, vol. 40, pp. 744-53.
37. I.C. Hsiao, S.W. Su, and J.C. Huang: *Metall. Mater. Trans. A*, 2000, vol. 31A, pp. 2169-80.
38. H. Watanabe, H. Tsutsui, T. Mukai, K. Ishikawa, Y. Okanda, M. Kohzu, and K. Higashi: *Mater. Sci. Forum*, 2000, vols. 350–351, pp. 171-76.
39. T. Mukai, H. Watanabe, and K. Higashi: *Mater. Sci. Forum*, 2000, vols. 350–351, pp. 159-64.
40. H. Watanabe, T. Mukai, T.G. Nieh, and K. Higashi: *Scripta Mater.* 2000, vol. 42, pp. 249-55.
41. T.G. Langdon: *Metall. Trans.*, 1972, vol. 3, pp. 797-801.
42. P. Shariat, R.B. Vastava, and T. Langdon: *Acta Metall.*, 1982, vol. 30, pp. 285-96.
43. U.F. Kocks, A.S. Argon, and M.F. Ashby: *Progr. Mater. Sci.*, 1975, vol. 19, pp. 110-70.
44. O.D. Sherby and J. Wadsworth: in *Deformation, Processing and Structure*, G. Krauss, ed., ASM, Metals Park, OH, 1984, pp. 355-65.
45. A. Ball and M.M. Hutchinson: *Met. Sci. J.*, 1969, vol. 3, pp. 1-7.
46. J. Weertman: *J. Appl. Phys.*, 1957, vol. 28, pp. 1185-89.
47. J. Harper and J.E. Dorn: *Acta Metall.*, 1957, vol. 5, pp. 654-65.
48. B. Burton: *Phil. Mag.*, 1972, vol. 25, pp. 645-59.
49. R.S. Mishra, T.R. Bieler, and A.K. Mukherjee: *Acta Metall. Mater.*, 1995, vol. 43, pp. 877-91.
50. K-T. Park and F.A. Mohamed: *Metall. Mater. Trans. A*, 1995, vol. 26A, pp. 3119-29.
51. H.J. Frost and M.F. Ashby: *Deformation-Mechanism Maps: the Plasticity and Creep of Metals and Ceramics*, Pergamon, New York, 1982, pp. 20-29.